JOC Article

Determination of the Absolute Configuration of Three *as*-Hydrindacene Compounds by Vibrational Circular Dichroism

T. Kuppens,[†] K. Vandyck,[‡] J. Van der Eycken,[‡] W. Herrebout,[§] B. J. van der Veken,[§] and P. Bultinck*,[†]

Department of Inorganic and Physical Chemistry, Ghent University, Krijgslaan 281-S3, B-9000 Gent, Belgium, Department of Organic Chemistry, Ghent University, Krijgslaan 281-S4, B-9000 Gent, Belgium, and Department of Chemistry, University of Antwerp, Groenenborgerlaan 171, B-2020 Antwerp, Belgium

patrick.bultinck@ugent.be

Received April 5, 2005

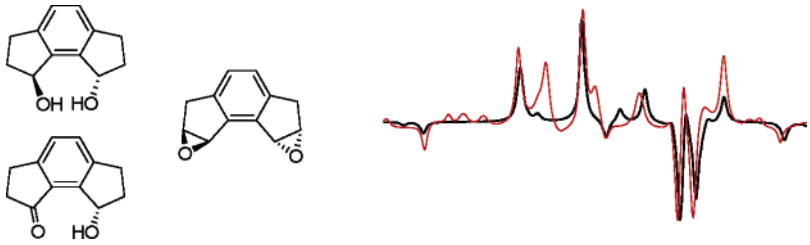

The absolute configurations of three compounds with a rigid 1,8-disubstituted *as*-hydrindacene skeleton have been determined using vibrational circular dichroism spectroscopy and quantum chemical calculations. Experimental spectra were compared to B3LYP/6-31G* and B3LYP/cc-pVTZ level predicted spectra. Based on the agreement between the predicted and experimental spectra, the stereochemistry could be assigned with high confidence. The results were found to be in agreement with ECD determinations and/or predictions based on the applied asymmetric methods in the synthetic route.

Introduction

Because the absolute configuration of molecules plays a dominant role in many fields of chemistry, methods to establish absolute configurations are of prime importance. One of the techniques that is continuously gaining more attention is the measurement of the vibrational circular dichroism (VCD). Essentially, VCD is based on the fact that when a molecule is irradiated with circularly polarized infrared radiation, different absolute configurations will exhibit different spectra. The most pictorial case is that of two enantiomers. Both enantiomers of a molecule will exhibit the same unpolarized infrared (IR) spectrum. When using circularly polarized IR radiation and measuring the spectrum with right and left circularly polarized light separately, the differential absorbance spectrum will exhibit mirror symmetry. Therefore, although the location of the absorbance peaks remains the same in VCD as in unpolarized IR spectra, in VCD the peaks have a different sign. As a result, a VCD spectrum contains information on the absolute configuration of a molecule. The interpretation of an experimental VCD spectrum and its connection with a specific stereochemistry has long remained a difficult task, however. A breakthrough was realized when Stephens et al. developed and implemented a quantum chemical algorithm for computing VCD spectra.[1−3] This has contributed greatly to the increasing popularity of the VCD technique. Essentially, one performs the necessary VCD calculations using some quantum chemical code for the different possible stereomers, and subsequently compares the resulting theoretical spectrum with the experimental one. Despite this conceptually simple approach, some problems remain in the routine application of VCD, so it remains important to check the outcome of the VCD assignments, if possible, with other ways of determining absolute configurations.[3−6] Some of the problems mentioned are related to the quantum chemical methodology

[†] Department of Inorganic and Physical Chemistry, Ghent University.
[‡] Department of Organic Chemistry, Ghent University.
[§] University of Antwerp.

(1) Cheeseman, J. R.; Frisch, M. J.; Devlin, F. J.; Stephens, P. J. *Chem. Phys. Lett.* **1996**, *252*, 211−220.
(2) Devlin, F. J.; Stephens, P. J.; Cheeseman, J. R.; Frisch, M. J. *J. Phys. Chem. A* **1997**, *101*, 9912−9924.
(3) Stephens, P. J.; Ashvar, C. S.; Devlin, F. J.; Cheeseman, J. R.; Frisch, M. J. *Mol. Phys.* **1996**, *89*, 579−594.
(4) Stephens, P. J.; Devlin, F. J.; Chabalowski, C. F.; Frisch, M. J. *J. Phys. Chem.* **1994**, *98*, 11623−11627.

10.1021/jo050666h CCC: $30.25
Published on Web 10/18/2005

used.[2,5,7−11] Density functional theory has previously been shown to give gratifying agreements between theory and experiment, but basis set effects can still play an important role.[7,12,13] The advent of commercially available VCD spectrometers and the implementation of the VCD algorithms in widely available software packages, together with the increase in speed and power of computers, will only extend the range of molecules that can be handled with the VCD technique.

In this paper, a vibrational circular dichroism (VCD) study on three 1,8-disubstituted *as*-hydrindacenes is presented, that is, (+)-1,2,3,6,7,8-hexahydro-*as*-indacene-1,8-diol ((+)-**1**), (+)-8-hydroxy-3,6,7,8-tetrahydro-2*H*-*as*-indacen-1-one ((+)-**2**), and $(-)_{365}$-1,2,7,8-di-epoxy-3,6-dihydro-*as*-indacene ((−)-**3**).[14] The VCD assignments are checked against stereochemistry information based on ECD measurements and/or predictions based on the applied asymmetric methods in the synthetic route.[15]

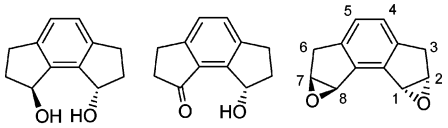

(1*S*,8*S*)-**1** (8*S*)-**2** (1*R*,2*S*,7*S*,8*R*)-**3**

Compounds **1**−**3** provide a chiral synthetic platform for the synthesis of a new class of rigid enantiopure hexahydro-*as*-indacene based chiral ligands for application in asymmetric catalysis.[16] The *as*-hydrindacenes can be viewed as C_2-symmetric analogues of Indane systems, which themselves have found numerous applications in asymmetric synthesis.

Derivatives of compounds **1** were recently studied with the circular dichroism exciton chirality method.[15] The determined absolute configurations of (+)-**1** and (+)-**2** are in agreement with what one would predict on the basis of the applied asymmetric reduction.

Results and Discussion

Synthesis. Asymmetric transfer hydrogenation of the C_2-symmetric prochiral diketone **4** applying an in situ prepared catalyst (**A**) derived from commercial (1*S*,2*S*)-(+)-*N*-*p*-tosyl-1,2-diphenylethylenediamine and $[RuCl_2(\eta^6\text{-cymene})]_2$ in a 5:2 formic acid-triethylamine mixture[17] resulted in alcohols (+)-**1** and (+)-**2** in good yield and high enantiomeric excess.[15] Depending on the catalyst loading, reaction time and reaction temperature, (+)-**1** or (+)-**2** could be isolated as the main product (Scheme 1). The reduction is expected to yield the (*S*)-alcohols using the (*S*,*S*)-Ts-DPEN ligand by analogy with the reduction of indanone to (*S*)-indanol with the same ligand. Furthermore, reduction of **4** with $NaBH_4$ in MeOH provided a 3/1 mixture of *meso*/(±)-**1** alcohols in 99% yield. Concentration-sensitive dehydration[18] in the presence of no more than 1% *p*-TSA yielded one C_2-symmetric isomer **5**. This prochiral alkene can be transformed into the bisepoxide **3** using the low-temperature Jacobsen epoxidation conditions.[19] Noteworthy is the isomerization of diene **5** by NMO at room temperature, emphasizing the importance of adding **5** at low temperature (−78 °C) to the mixture of catalyst and NMO, not at room temperature. The use of the (*R*,*R*)-catalyst allows one to predict the absolute configuration to be (1*R*,2*S*) deduced from the formation of (1*S*,2*R*)-indene oxides when using the (*S*,*S*)-Jacobsen catalyst.[20,21]

SCHEME 1

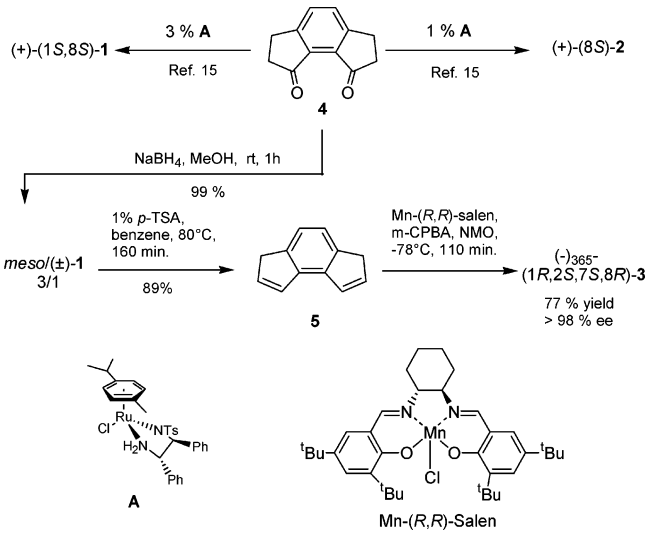

Conformational Analysis. Hexahydro-*as*-indacene-1,8-diol (1). Molecule **1** has two asymmetric carbon atoms. Because the sample of (+)-**1**, which is analyzed, is optically active (>99% ee), the possible configurations of (+)-**1** are limited to enantiomers $\mathbf{1}^{(RR)}$ or $\mathbf{1}^{(SS)}$ (mesomers $\mathbf{1}^{(RS)}$ and $\mathbf{1}^{(SR)}$ are identical and not optically active).

The conformational space can be described by means of the orientation of the exocyclic substituents. The position of the alcohol group in context of the five-membered ring is either designated as equatorial ("e") or axial ("a"). For the C−O(*H*) bond torsion, three typical

(5) Stephens, P. J. Vibrational circular dichroism spectroscopy: A new tool for the stereochemical characterization of chiral molecules. In *Computational medicinal chemistry for drugs discovery*; Bultinck, P., De Winter, H., Langenaeker, W., Tollenaere, J. P., Eds.; Marcel Dekker: New York, 2004; pp 699−725.
(6) Wang, F.; Wang, Y.; Polavarapu, P. L.; Li, T. Y.; Drabowicz, J.; Pietrusiewicz, K. M.; Zygo, K. *J. Org. Chem.* **2002**, *67*, 6539−6541.
(7) Kuppens, T.; Langenaeker, W.; Tollenaere, J. P.; Bultinck, P. *J. Phys. Chem. A* **2003**, *107*, 542−553.
(8) Aamouche, A.; Devlin, F. J.; Stephens, P. J.; Drabowicz, J.; Bujnicki, B.; Mikolajczyk, M. *Chem.-Eur. J.* **2000**, *6*, 4479−4486.
(9) Aamouche, A.; Devlin, F. J.; Stephens, P. J. *J. Am. Chem. Soc.* **2000**, *122*, 2346−2354.
(10) Polavarapu, P. L.; Zhao, C. X.; Ramig, K. *Tetrahedron: Asymmetry* **1999**, *10*, 1099−1106.
(11) Wang, F.; Polavarapu, P. L.; Lebon, F.; Longhi, G.; Abbate, S.; Catellani, M. *J. Phys. Chem. A* **2002**, *106*, 5918−5923.
(12) Freedman, T. B.; Cao, X. L.; Dukor, R. K.; Nafie, L. A. *Chirality* **2003**, *15*, 743−758.
(13) Stephens, P. J.; Devlin, F. J. *Chirality* **2000**, *12*, 172−179.
(14) (+)-**1**: $[\alpha]_D^{20} = +70.5$ (*c* 1.09, $CHCl_3$, >99% ee). (+)-**2**: $[\alpha]_D^{25} = +98.2$ (*c* 1.04, $CHCl_3$, >99% ee). $(-)_{365}$-**3**: $[\alpha]_{365}^{25} = -128.6$ (*c* 0.99, $CHCl_3$, >99% ee).
(15) Vandyck, K.; Matthys, B.; Van der Eycken, J. *Tetrahedron Lett.* **2005**, *46*, 75−78.
(16) *Catalytic Asymmetric Synthesis*; Ojima, I., Ed.; Wiley-VCH: New York, 2000.
(17) Fujii, A.; Hashiguchi, S.; Uematsu, N.; Ikariya, T.; Noyori, R. *J. Am. Chem. Soc.* **1996**, *118*, 2521−2522.
(18) Moglioni, A. G.; Tombari, D. G.; Iglesias, G. Y. M. *J. Chem. Res., Synop.* **1998**, 606−607.
(19) Palucki, M.; Pospisil, P. J.; Zhang, W.; Jacobsen, E. N. *J. Am. Chem. Soc.* **1994**, *116*, 9333−9334.
(20) Kobayashi, T.; Tanaka, K.; Miwa, J.; Katsumura, S. *Tetrahedron: Asymmetry* **2004**, *15*, 185−188.
(21) Larrow, J. F.; Roberts, E.; Verhoeven, T. R.; Ryan, K. M.; Senanayake, C. H.; Reider, P. J.; Jacobsen, E. N. *Org. Synth.* **1999**, *76*, 46−56.

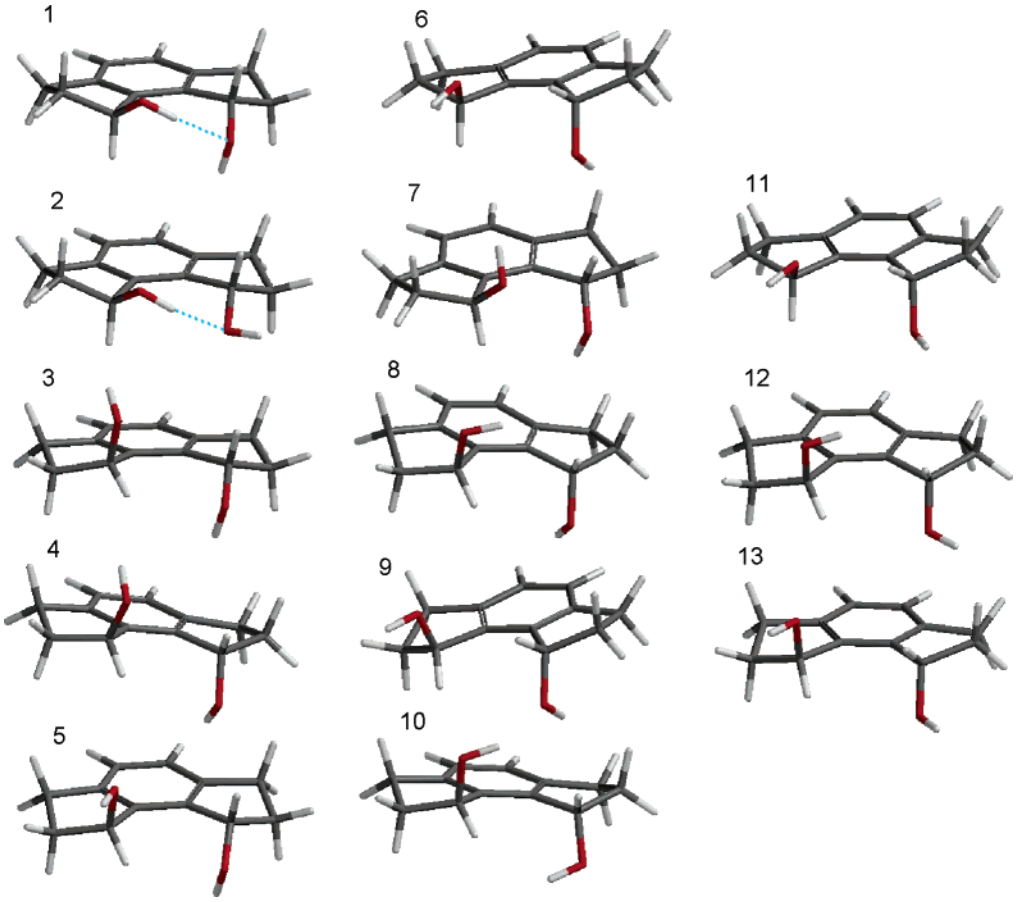

FIGURE 1. Pictorial representation of the B3LYP/6-31G* PES minima for **1**. Conformation numbering conforms to that of Table 1.

minima in the torsion potential energy are observed, that is, for dihedral angles of 60°, 180°, and −60°. The dihedral angles are characterized as G, T, and G′, respectively, for gauche clockwise, trans, and gauche counterclockwise.

Due to the C_2-symmetry of **1**, both substituents are indistinguishable, which is reflected in the conformational notation; the group-ring orientation and C−O(*H*) bond torsion are given successively for both functional groups. In this fashion, the global minimum of **1** can be written as eG′eG or eGeG′.

The combined conformational searches, using different techniques that are described in the Methods section, yielded 13 minima in total. These minima are shown in Figure 1.

Their corresponding notation and energy can be found in Table 1. For each minimum, the B3LYP 6-31G* and cc-pVTZ relative total energies are given. Some higher energy cc-pVTZ conformers have a different energy order as compared to the 6-31G*. Also, the expected eTaG minimum could not be located at B3LYP/cc-pVTZ level. Starting from the B3LYP/6-31G* eTaG geometry, cc-pVTZ optimization converged in the eG′eG structure. Conformational populations are calculated on the basis of the Boltzmann distribution using free energies at 298.15 K. From Table 1, it is clear that eG′eG and eG′eT are dominant minima, the populations of both conformers being more than 90%. This can be attributed to two effects, that is, an internal OH···O hydrogen bond and the gauche effect.[22] This stabilization is more pronounced for the 6-31G* basis set.

Hydroxy-tetrahydro-*H*-*as*-indacen-one (2). In hydroxyketone **2**, only one group-ring orientation and C−O(*H*) bond torsion is present; a notation from compound **1** is used. A combined stochastic MM3 and systematic MMFF search resulted in three B3LYP/6-31G* minima. These are shown in Figure 2 and listed in Table 2 accompanied with the 6-31G* and cc-pVTZ relative energies, enthalpies, free energies, and Boltzmann populations. Remarkably, the expected minima eT, aT, and aG′ are not found. Therefore, a B3LYP/6-31G* systematic search around the C−C−O−H dihedral angle for an equatorial and axial substitution is performed. In Figure 3, the 2D PES is shown for the equatorial and axial scan, whereas the C−C−O−H torsion is varied in steps of 1° and is held fixed during optimization. As can be seen, no new minima are encountered. A transition from the axial surface to the equatorial surface can be observed in the proximity of the global minimum. This minimum is stabilized due to a strong internal OH···O hydrogen bond (1.95 Å − B3LYP/cc-pVTZ).

Di-epoxy-dihydro-*as*-indacene (3). Because the four stereocentra of **3** are in a ring-attached epoxide system, they are two-by-two correlated. Due to the optical activity of the molecule, only the enantiomers $\mathbf{3}^{(RS,SR)}$ and $\mathbf{3}^{(SR,RS)}$ are likely.

(22) Wolfe, S. *Acc. Chem. Res.* **1972**, *5*, 102−111.

TABLE 1. The B3LYP/6-31G* (A) and B3LYP/cc-pVTZ (B) Relative Energies for the Localized Conformations (RE, in kcal/mol) of 1, the Conformation Description, Relative Enthalpies (Δ*H*°, in kcal/mol), Relative Free Energies (Δ*G*°, in kcal/mol), and the Boltzmann Populations (%F, *T* = 298.15 K)

A	notation	RE	Δ*H*°	Δ*G*°	%F
1	eG′eG	0.00	0.00	0.00	84.11
2	eG′eT	1.10	1.05	1.05	14.31
3	aGeG	4.42	4.16	3.20	0.38
4	aGaG	4.50	4.24	3.47	0.24
5	aTeG	4.89	4.57	3.61	0.19
6	eTaG	5.01	4.66	4.13	0.08
7	eGeG	4.97	4.68	3.46	0.24
8	aGaG′	5.14	4.82	3.64	0.18
9	aTaG	5.18	4.87	3.76	0.15
10	aG′aG′	5.84	5.40	4.72	0.03
11	eTaT	5.89	5.48	4.42	0.05
12	aG′aT	6.22	5.80	5.18	0.01
13	aTaT	6.19	5.81	4.74	0.03
B	notation	RE	Δ*H*°	Δ*G*°	%F
1	eG′eG	0.00	0.00	0.00	71.31
2	eG′eT	0.78	0.73	0.73	20.72
4	aGaG	3.20	3.07	2.49	1.07
3	aGeG	3.35	3.19	2.29	1.50
5	aTeG	3.68	3.44	2.43	1.19
8	aGaG′	3.73	3.52	2.43	1.17
9	aTaG	3.74	3.52	2.47	1.10
6	eGeG	4.02	3.82	3.25	0.29
11	eTaT	4.28	3.94	3.11	0.37
10	aG′aG′	4.29	3.93	0.10	0.59
12	aTaT	4.58	4.26	0.06	0.32
13	aG′aT	4.65	4.28	0.06	0.38

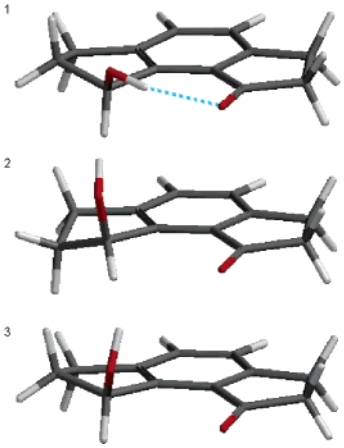

FIGURE 2. Pictorial representation of the B3LYP/6-31G* PES minima for **2**. Conformation numbering conforms to that of Table 2.

Due to the rigidity of compound **3**, only one conformation could be found (depicted in Figure 4) using a stochastic and systematic MM search, as described in the Methods section.

IR and VCD Spectra. In Figures 5 and 6, the Lorentzian fitted experimental IR and VCD spectra of (+)-**1** are given (residual fitting errors are given in Figure S12 − Supporting Information available). From the Boltzmann populations in Table 1, it can be seen that only two conformations have a considerable contribution. All conformations, however, are taken into account to simulate the spectra. Only eG′eG and eG′eT are needed to assign the experimental bands. Fundamentals designated as *a* originate from conformation eG′eG; those designated as *b* represent eG′eT. No label is used when fundamentals of both conformations coincide or have a very small frequency separation.

TABLE 2. The B3LYP/6-31G* (A) and B3LYP/cc-pVTZ (B) Relative Energies for the Localized Conformations (RE, in kcal/mol) of 2, the Conformation Description, Relative Enthalpies (Δ*H*°, in kcal/mol), Relative Free Energies (Δ*G*°, in kcal/mol), and the Boltzmann Populations (%F, *T* = 298.15 K)

A	notation	RE	Δ*H*°	Δ*G*°	%F
1	eG′	0.00	0.00	0.00	100.00
2	aG	6.85	6.59	5.75	0.00
3	eG	8.19	7.87	6.75	0.00
B	notation	RE	Δ*H*°	Δ*G*°	%F
1	eG′	0.00	0.00	0.00	99.97
2	aG	5.97	5.73	4.90	0.03
3	eG	7.41	7.17	6.03	0.00

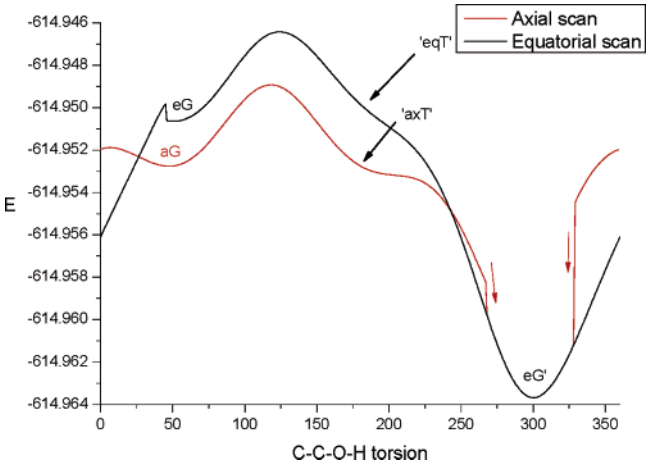

FIGURE 3. PES scan (C−C−O−H torsion) at B3LYP/6-31G* level of the equatorial and axial surface of **2** in steps of 1°. The torsion is held fixed during optimization. Energies are in hartrees.

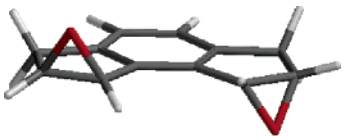

FIGURE 4. Pictorial representation of the B3LYP/6-31G* PES minimum for **3**.

In Figures 5 and 6, the simulated spectra are shown for (1*S*,8*S*)-**1**. The B3LYP/6-31G* theoretical frequencies are uniformly scaled with a factor of 0.967; the B3LYP/cc-pVTZ spectra are scaled with a factor 0.977.

The experimental assignments could be performed relatively easy due to the good agreement between theory and experiment, although peak broadening makes the assignment of the low intensity peaks (38−52) somewhat less straightforward. The peak assignment is primarily based on the IR spectrum. Nevertheless, due to the extra discriminating power provided by VCD, that is, the intensity sign, some unresolved IR bands could be localized, because of their corresponding resolved VCD bands.

In the experimental IR absorption spectrum, fundamentals 48 and 57 are not clearly visible. Fundamentals

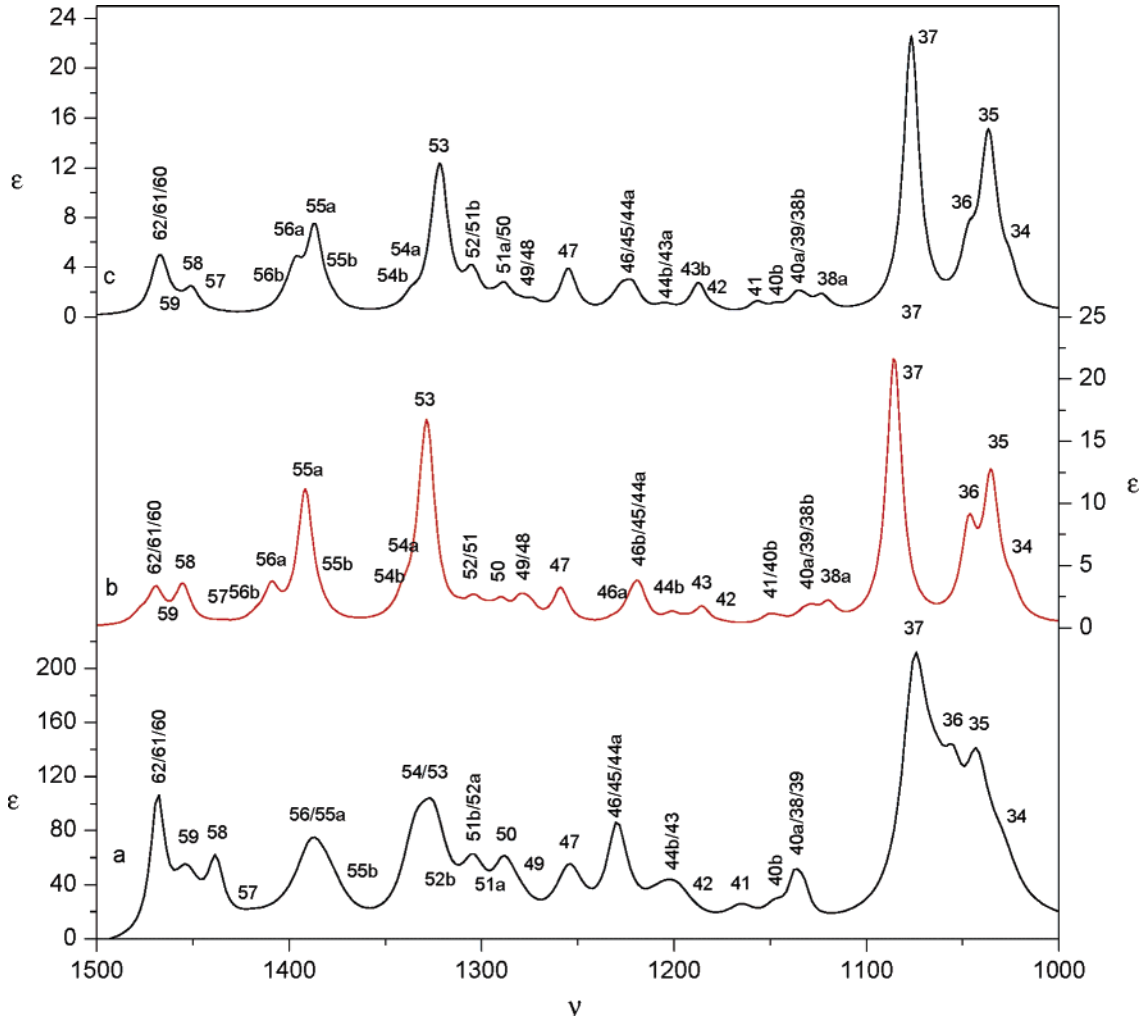

FIGURE 5. Lorentzian fitted unpolarized IR absorption spectrum for the (+)-**1** (a), B3LYP/6-31G* (b), and B3LYP/cc-pVTZ (c) simulated IR spectrum for (1*S*,8*S*)-**1**. Experimental intensities in absorbance units and theoretical intensities in 10^{-40} esu^2 cm^2; frequencies in cm^{-1}.

44b/43, 55b, and 56/55a are not well resolved. Fundamentals 40a/38/39, 46/45/44a, and 62/61/60 are not resolved either, but their predicted frequency separations are also very small. In the experimental VCD spectrum, peak 56b is not well resolved, and peak 48 is not visible.

In Figure 6, there is clearly a difference in sign for fundamental 37 as compared to the 6-31G* spectrum. In the cc-pVTZ spectrum, however, the peak is predicted with the correct sign, but is strongly underestimated. The better agreement with the cc-pVTZ basis set is coherent with earlier studies.[7] Other functionals (B1LYP, B3P86, B3PW91, B98, MPW1PW91, PBE1PBE, BHandH, BHandHLYP) are also used along with the 6-31G* basis set to simulate spectra for **1**. It seems that only the B1LYP functional predicts the correct sign for fundamental 37. This functional also predicts fundamental 54, which is experimentally not resolved, to be positive in agreement with the cc-pVTZ basis set. When looking at the overall performance of the various functionals, only BHandH and BHandHLYP perform rather poorly. The other functionals have a comparable performance. The B3LYP functional has the best overall agreement. In Table S14/A (Supporting Information), the neighborhood overlap (eq 2) between experimental and simulated IR/VCD spectra is given. This type of overlap takes the local shift of the simulated band with respect to the experimental one into account, even when calculated frequencies are uniformly scaled. In addition, the scaling factor is given for which the normalized overlap between experimental and simulated IR spectra is maximized. The overlap is calculated for the 1700−1000 cm^{-1} wavenumber interval.

For **1**, intermolecular interactions with solvent or solute molecules via the OH groups, which could perturb the spectra notably, are possible.[23] These interactions are not taken into account in our calculations, as these are performed on isolated molecules. In Figure 7, the IR spectra in the OH stretch region for four different concentrations are given, that is, 0.11 M (saturated solution), 81 mM, 48 mM, and 32 mM. Two OH stretch bands can be observed, that is, an unresolved doublet due to noninteracting OH groups, and a doublet at 3589 cm^{-1} caused by the OH stretching fundamental involved in OH···O intramolecular hydrogen bonds. Doublets are due to the two most significant conformations. Figure 7 also

(23) He, J. T.; Polavarapu, P. L. *Spectrochim. Acta, Part A* **2005**, *61*, 1327−1334.

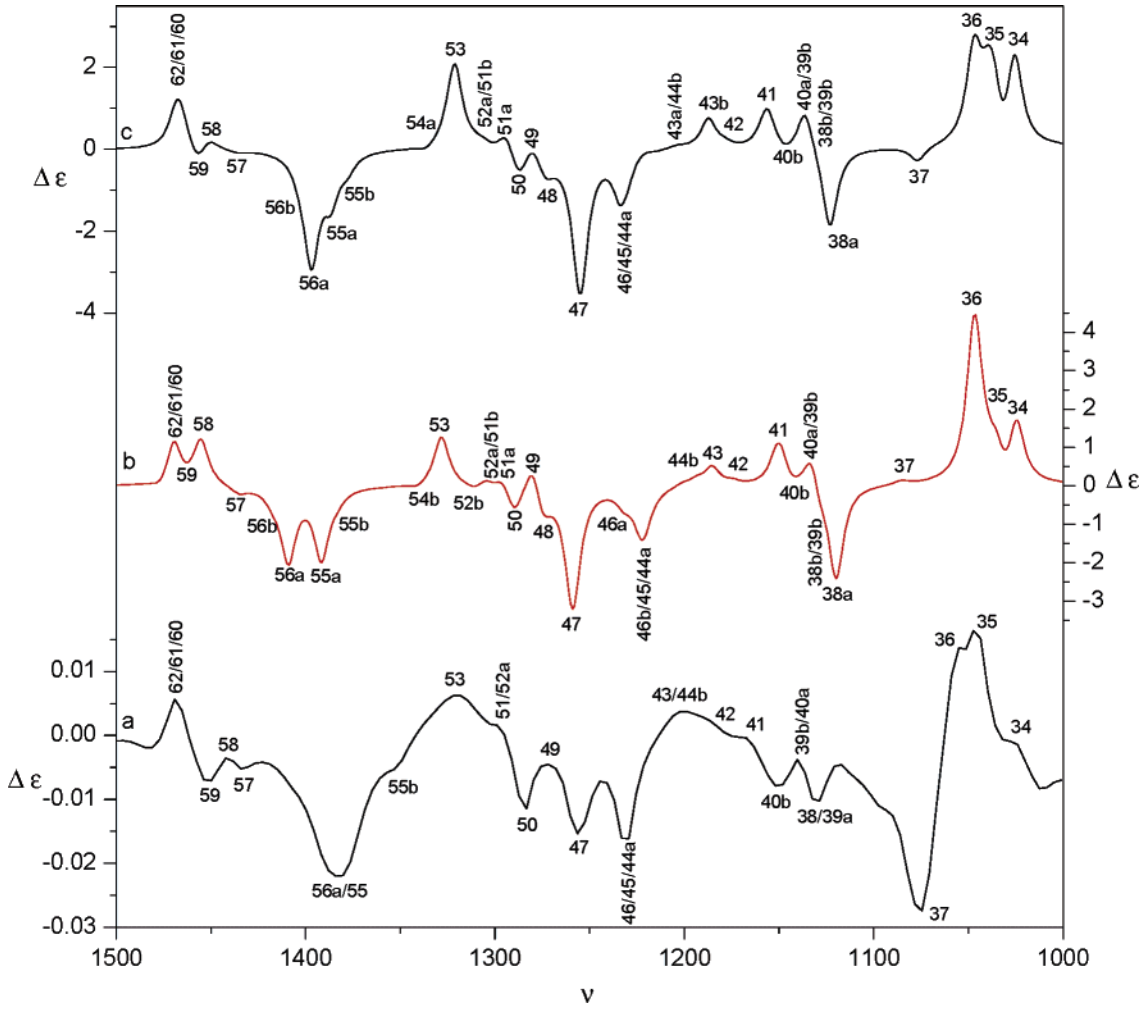

FIGURE 6. (a) Lorentzian fitted experimental VCD spectrum for the (+)-**1** (a), B3LYP/6-31G* (b), and B3LYP/cc-pVTZ (c) simulated VCD spectrum for (1*S*,8*S*)-**1**. Experimental differential intensities in absorbance units and theoretical intensities in 10^{-44} esu^2 cm^2; frequencies in cm^{-1}.

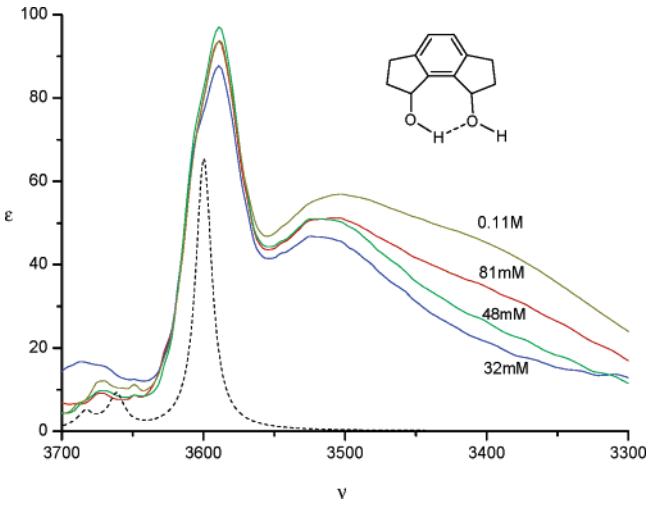

FIGURE 7. Infrared spectrum in the OH stretch region for different concentrations of **1** (0.11 M, 81 mM, 48 mM, and 32 mM). The dashed line is the B3LYP/6-31G* simulated spectrum. Experimental intensities are in absorbance units; frequencies in cm^{-1}.

contains the B3LYP/6-31G* simulated spectrum. The predicted frequencies for the OH stretching fundamental in the OH···O intramolecular hydrogen bond in conformations eG′eG and eG′eT nearly coincide, giving rise to only one peak. The broad band at 3513 cm^{-1} is due to self-association (hydrogen bonding between different solute molecules). The intensity of this band becomes somewhat smaller with lower concentrations. Comparing its intensities to those of the two monomeric bands, however, it is clear that self-association is less important. Furthermore, there is no concentration effect observed for the VCD spectra of the concentration series.

Given the excellent agreement between the experimental and simulated spectra, the absolute configuration of (+)-**1** can be assigned as (1*S*,8*S*)-**1**. This is in agreement with earlier ECD studies.[15]

In Figures 8 and 9, the Lorentzian fitted experimental IR and VCD spectra of (+)-**2** are shown (residual fitting errors are given in Figure S12 − Supporting Information) simultaneously with the B3LYP/6-31G* and B3LYP/cc-pVTZ simulated spectra for the *S* enantiomer of compound **2**. The 6-31G* and cc-pVTZ frequency scale factors that are used are 0.967 and 0.977, respectively. Based on the populations (Table 2), it can be seen that only conformation eG′ should be considered when assigning the peaks in the experimental spectrum. This as-

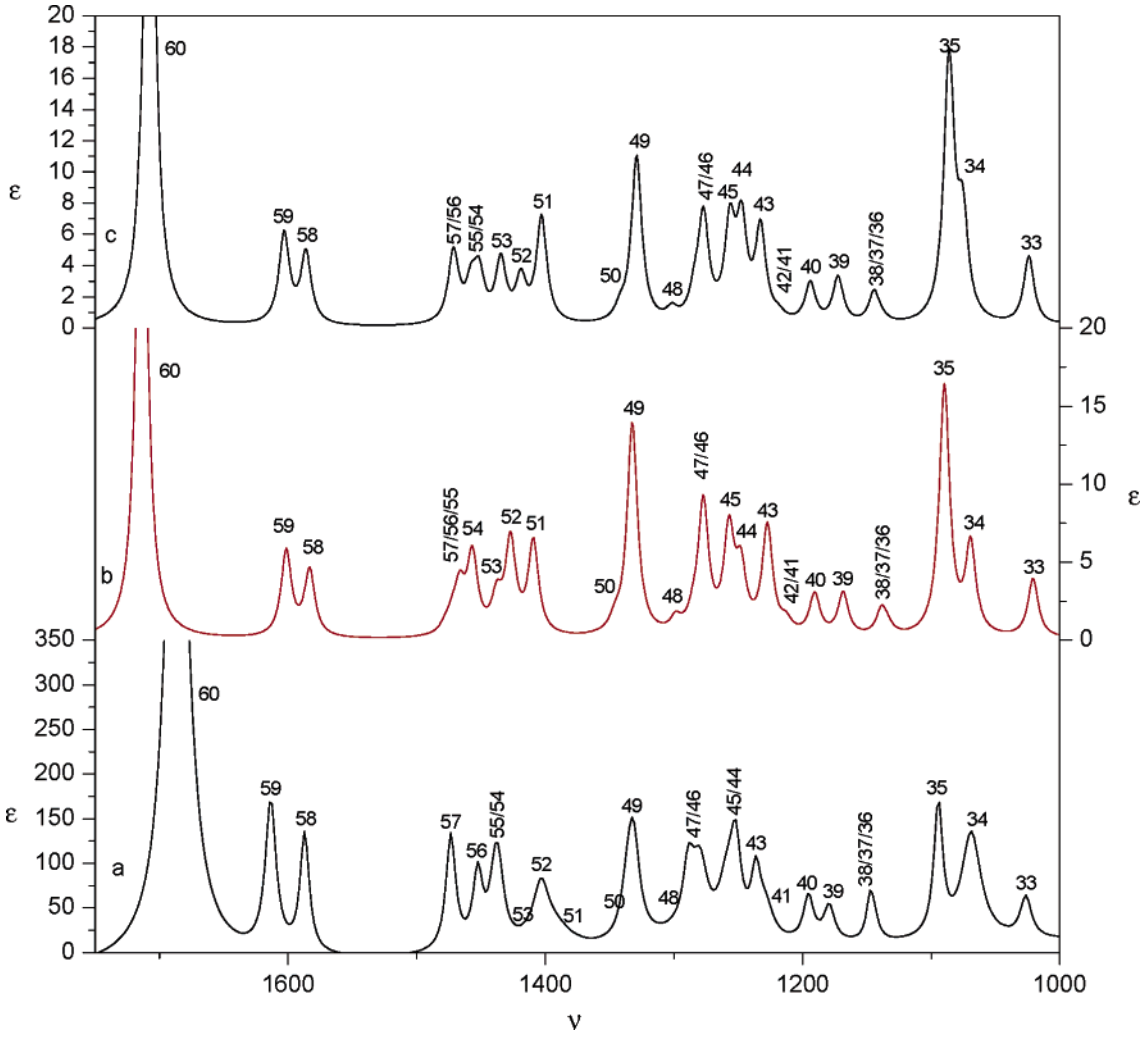

FIGURE 8. Lorentzian fitted unpolarized IR absorption spectrum for the (+)-**2** (a), B3LYP/6-31G* (b), and B3LYP/cc-pVTZ (c) simulated IR spectrum for *S*-**2**. Experimental intensities in absorbance units and theoretical intensities in 10^{-40} esu^2 cm^2; frequencies in cm^{-1}.

signment was based on the 6-31G* and cc-pVTZ calculations.

In the experimental IR spectrum, it can be seen that peaks 36/37/38, 45/44, and 54/55 are not resolved, in agreement with the predicted small frequency separation. Peaks 53, 51, 50, and 42 are not visible.

In the experimental VCD spectrum, peaks 46/47 and 38/37 are not resolved, in agreement with simulations. Peaks 58, 53, and 42 are not visible.

When looking at the signs of the VCD peaks for (+)-**2** in Figure 9, it can be judged that the sign of fundamental 35 is not correctly predicted for both basis sets. For 6-31G* fundamentals, 56 and 57 have the wrong predicted sign. For the cc-pVTZ simulated spectra, fundamental 59 is erroneously predicted, that is, slightly positive. However, predicted VCD intensities for fundamental 59 are very small, and the noise level in that area of the experimental spectrum is rather high.

Different functionals are used to simulate spectra at 6-31G* level. None of the functionals manage to correctly predict the sign for fundamental 35. B3P86, MPW1PW91, and PBE1PBE succeed in calculating the correct signs for fundamentals 57 and 56 but fail for fundamental 55. In an overview of the overall performance of the different functionals, Table S14/B (Supporting Information) gives the neighborhood overlap for experimental and simulated IR/VCD spectra, along with the scaling factor. It shows again that, for our purposes, BHandH and BHandHLYP have a bad performance at the 6-31G* level. The other functionals perform similarly.

In the OH stretch region, three distinct bands can be observed: one band at 3672 cm^{-1}, a small shoulder at 3594 cm^{-1}, and a broad asymmetric band at 3430 cm^{-1}. In agreement with the B3LYP/6-31G* force field calculations, the OH stretch band for the intramolecular hydrogen-bonded system is shifted to a lower wavenumber and can be found at approximately 3430 cm^{-1} (Figure 10). This band is asymmetric and relatively broad. As can be seen, there is no concentration effect, meaning that this broadening cannot be attributed to self-association, as diluting affects the aggregation. However, $CDCl_3$ solvent molecules can interact with the solute (CCl_3–D···O(H)–C), further reducing the OH stretch frequency. This was confirmed at the B3LYP/6-31G* level, taking this interaction explicitly into account (Figure 10). In this manner, the asymmetric broad band can be explained. The band at 3672 cm^{-1} and its small shoulder can be explained by taken into account the conformations without intramo-

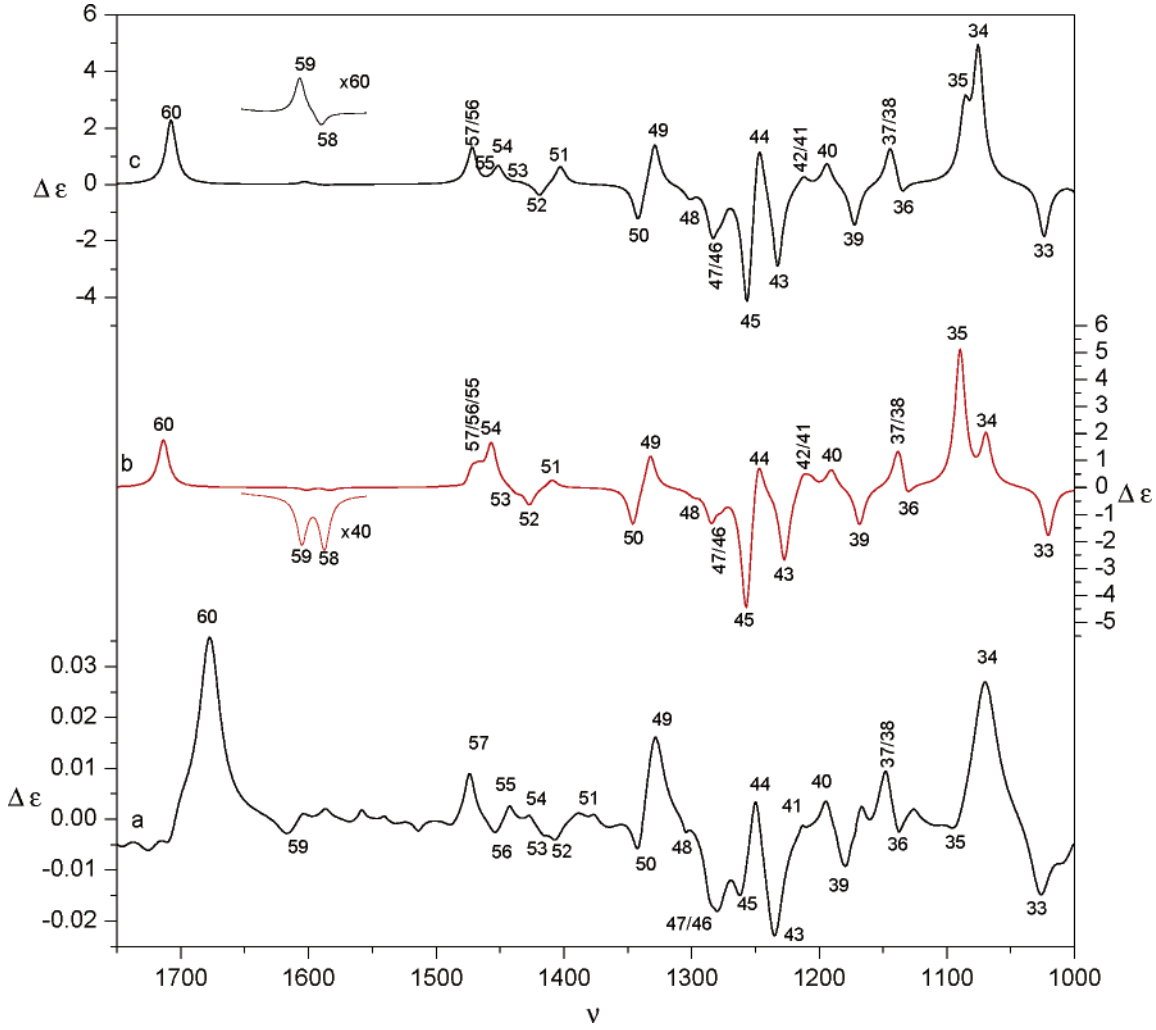

FIGURE 9. Lorentzian experimental VCD spectrum for the (+)-**2** (a), B3LYP/6-31G* (b), and B3LYP/cc-pVTZ (c) simulated VCD spectrum for *S*-**2**. Experimental differential intensities in absorbance units and theoretical intensities in 10^{-44} esu^2 cm^2; frequencies in cm^{-1}.

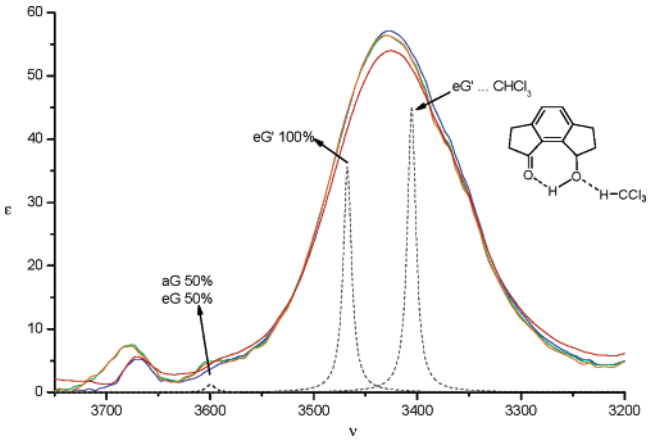

FIGURE 10. Infrared spectrum in the OH stretch region for different concentrations of **2** (0.19 M, 0.14 M, 95 mM, and 57 mM). The dashed lines are B3LYP/6-31G* simulated spectra. Experimental intensities are in absorbance units; frequencies in cm^{-1}.

lecular hydrogen bonding. Based on gas-phase calculations, their contributions are insignificant as compared to the global minimum (Table 2), but due to solvent stabilization these conformations apparently gain importance. More evidence can be found at the C=O stretch region, where a doublet is observed in the VCD spectrum (Figure 9, fundamental 60). However, the relative intensities of these stabilized conformation bands are low as compared to those of the intramolecular hydrogen bonds. Calculations in which the experimental spectrum was reproduced by averaging the calculated VCD spectra and manual adjustment of the conformational populations show that the experimental spectra are largely dominated by the global minimum eG′.

For the C−O(H) stretching mode, fundamental 35, the calculations always yield a positive VCD signal, while the experimental data clearly show that for this mode a negative signal is present. A similar pattern is also observed for fundamental 37 in **1**. The B3LYP/6-31G* calculations for this species give a wrong sign for fundamental 37. The calculations using the cc-pVTZ basis set yield a correct sign, but seriously underestimated the rotational strength.

The agreement for some areas is not as excellent as for **1**, but the overall agreement allows one to conclude with certainty that the absolute configuration of (+)-**2** corresponds to (8*S*)-**2**. This is in agreement with the

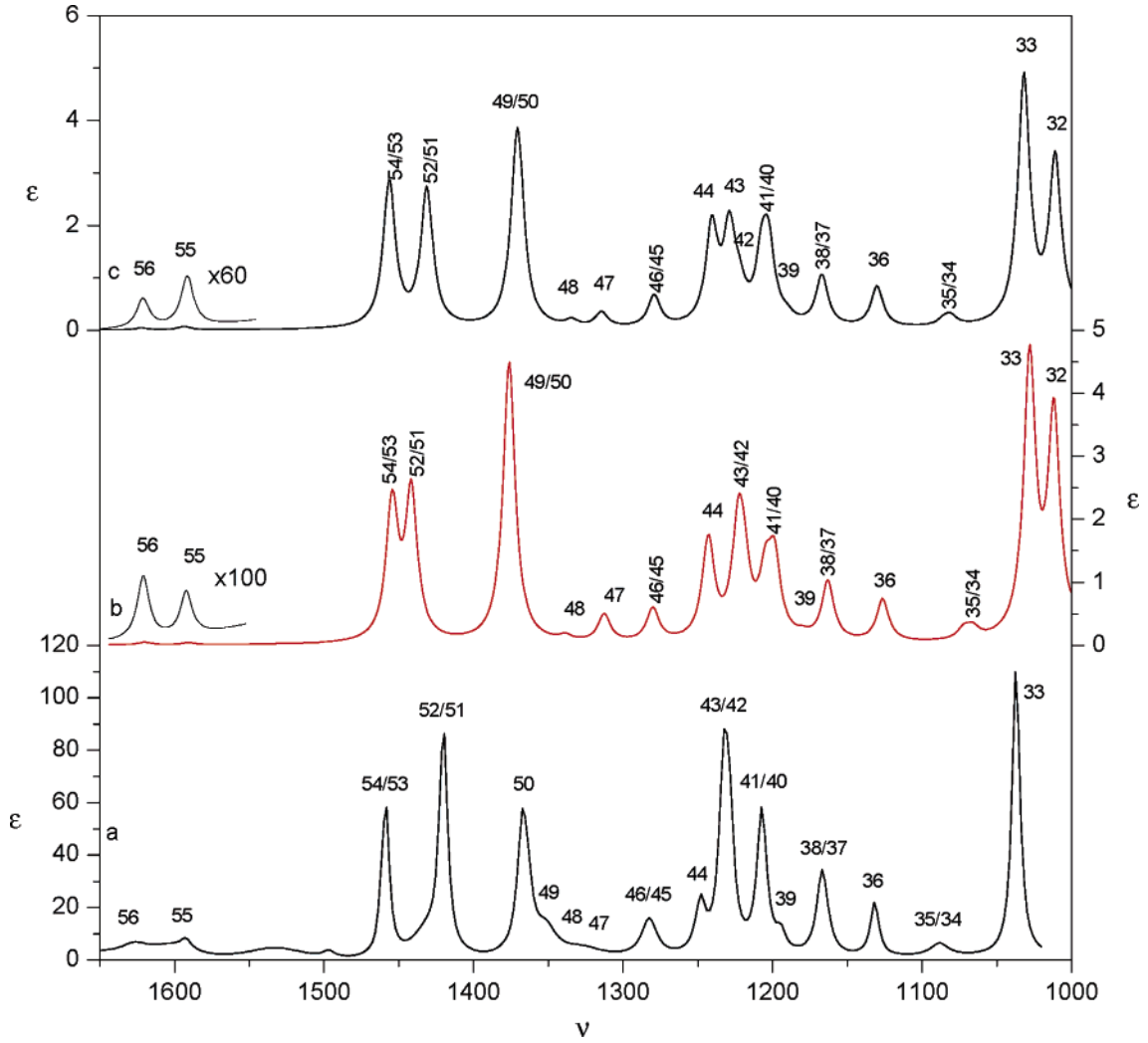

FIGURE 11. Lorentzian fitted unpolarized IR absorption spectrum for the (−)-**3** (a), B3LYP/6-31G* (b), and B3LYP/cc-pVTZ (c) simulated IR spectrum for (1*R*,2*S*,7*S*,8*R*)-**3**. Experimental intensities in absorbance units and theoretical intensities in 10^{-40} esu^2 cm^2; frequencies in cm^{-1}.

earlier ECD exciton chirality assignment and the prediction based on the selectivity of the asymmetric reduction of indanone with the same catalyst.[15]

In Figures 11 and 12, the Lorentzian fitted experimental IR and VCD spectra of (−)-**3** are given (residual fitting errors are given in Figure S12 − Supporting Information). Also, the simulated spectra are shown for (1*R*,2*S*,7*S*,8*R*)-**3**. The B3LYP/6-31G* theoretical frequencies are uniformly scaled with a factor of 0.967; the B3LYP/cc-pVTZ spectra are scaled with a factor 0.977.

The assignment of the fundamentals was relatively easy because only one conformation is to be taken into account, thereby reducing the complexity of the spectrum and assignment.

For the experimental spectra of (−)-**3**, peak 32 is not visible. Peaks 54/53, 46/45, 43/42, 41/40, 38/37, and 35/34 are not good resolved, in agreement with the predicted small frequency splitting. Peaks 47 and 48 give measurable VCD but are not resolved. The broad left shoulder of the peak labeled 52/51 is presumably attributable to fundamental 52.

In the VCD spectrum, peaks 56 and 47 are not well resolved.

Comparing the experimental and B3LYP/6-31G* VCD data (Table S22, Supporting Information), it can be seen that fundamentals 49 and 51 have wrong predicted signs. For the cc-pVTZ basis set, fundamental 51 has still the wrong predicted sign. Fundamental 50 is also wrongly predicted. These discrepancies, however, can only be seen when comparing the rotational strengths and not in the broadened spectra because of the small frequency separations between modes 49/50 and 51/52 (Table S22/S23, Supporting Information). Comparing the calculated rotational strengths for different functionals, it shows that fundamental 49 is predicted to have a wrong (negative) sign. The functionals that predict the sign of fundamental 51 correctly (B3P86, B3PW91, MPW1PW91, and PBE1PBE) fail to predict the sign correctly for fundamentals 44 and 52. All functionals have a comparable performance, apart from BHandH and BHandHLYP, which have a bad performance. In Table S14/C (Supporting Information), this is shown through the neighborhood overlap values between simulation and experiment.

Comparing experimental spectra with simulated spectra, we can see an excellent agreement, allowing an

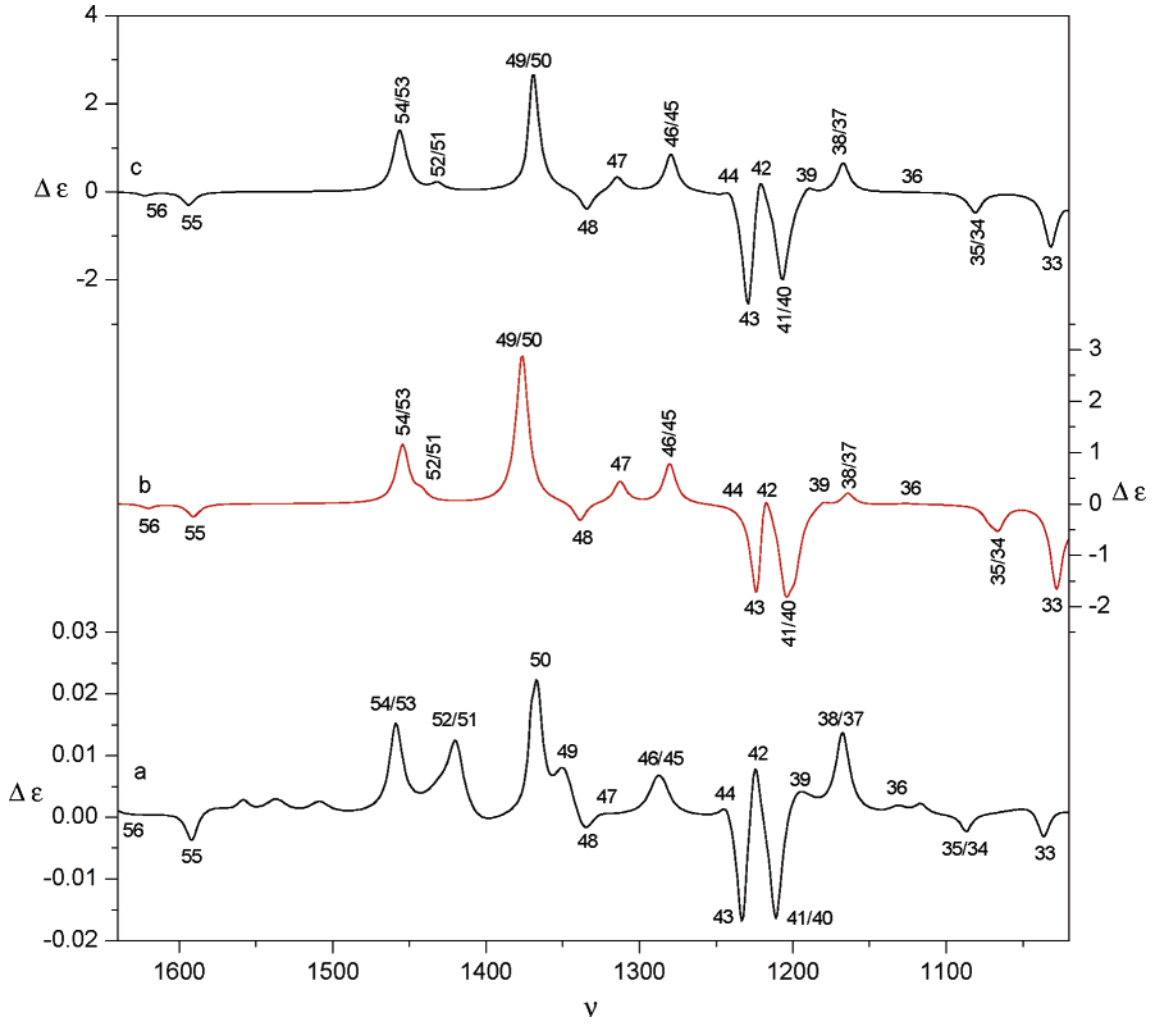

FIGURE 12. Lorentzian fitted experimental VCD spectrum for the (−)-**3** (a), B3LYP/6-31G* (b), and B3LYP/cc-pVTZ (c) simulated VCD spectrum for (1*R*,2*S*,7*S*,8*R*)-**3**. Experimental differential intensities in absorbance units and theoretical intensities in 10^{-44} esu^2 cm^2; frequencies in cm^{-1}.

TABLE 3. Neighborhood Similarity S_{fg} for IR and VCD Spectra for Theory versus Experiment for (A) 6-31G* and (B) cc-pVTZ Basis Sets

A	S_{fg} IR	S_{fg} VCD
1	0.957	0.830
2	0.968	0.882
3	0.952	0.800
B	**S_{fg} IR**	**S_{fg} VCD**
1	0.978	0.857
2	0.983	0.917
3	0.964	0.851

assignment of the absolute configuration of (−)-**3** to (1*R*,2*S*,7*S*,8*R*)-**3**.

Comparing the performance of the basis sets for the three molecules, it shows again[7,13] that 6-31G* is adequate to perform absolute configuration assignments, with the cc-pVTZ basis set being superior. This is shown in the above discussion, but is also clear from Table 3, where the neighborhood overlap (eq 2) is given between experimental IR/VCD spectra and the simulated spectra. The cc-pVTZ neighborhood overlap values are all closer to 1 as compared to the 6-31G* values, indicating a better agreement with experiment.

Conclusion

Absolute configurations of (+)-**1**, (+)-**2**, and $(-)_{365}$-**3** were determined respectively as (1*S*,8*S*)-**1**, (8*S*)-**2**, and (1*R*,2*S*,7*S*,8*R*)-**3**. This was accomplished on the B3LYP/6-31G* and cc-pVTZ levels. cc-pVTZ spectra were proven to be superior to the 6-31G* spectra, which confirms earlier studies. Also, it is shown that small differences between theory and experiment are not the effect of the choice of functional, as the performance of most functionals is very comparable.

The use of VCD to assign absolute configurations is a powerful method, which allows the determination of the absolute configurations based on quantum chemical calculations and experimental spectra of dilute solutions. In contrast to the ECD determination for compounds **1** and **2**, the VCD method does not require extra synthesis steps to introduce chromophore groups to induce exciton coupling.

Methods

Mixture of *meso*/(±)-1,2,3,6,7,8-Hexahydro-*as*-indacene-1,8-diol: *meso*/(±)-1. A suspension of diketone **4** (5.06 g, 27.2 mmol) was stirred in MeOH (150 mL) at 0 °C, and $NaBH_4$ was

added (1.03 g, 27.2 mmol) in several portions in such a way that the temperature did not exceed 10 °C. The mixture was then stirred at room temperature for 1 h, after which it was poured into H_2O (350 mL) and EtOAc (400 mL). The aqueous layer was separated and again extracted with EtOAc (2 × 400 mL). The organic layer was washed with saturated aqueous NaCl and dried with Na_2SO_4. Filtration and removal of the solvent in vacuo resulted in 5.12 g (26.9 mmol, 99%) of a 3/1 mixture *meso*/(±)-**1** as a white solid.

R_f ((±)-**1**): 0.20 (toluene/*i*PrOH 95:5). R_f (*meso*): 0.29 (toluene/*i*PrOH 95:5). The ratio *meso*/(±)-**1** was determined by integration of the ^{1}H-aromatic signals *meso* δ = 7.14 (2H, s) ppm, (±)-**1** δ = 7.10 (2H, s) ppm and confirmed by reversed phase HPLC: Phenomenex Luna (2) C18 4.6 × 250 mm 5 μm, H_2O (5 mM NH_4OAc)/CH_3CN 70/30, retention times **4** = 5.2 min, (±)-**1** = 7.3 min, (±)-**2** = 13.0 min, *meso*-**1** = 13.8 min.

3,6-Dihydro-*as*-indacene 5. The *meso*/(±)-**1** 3/1 mixture (5.12 g, 26.9 mmol) was dissolved in dry benzene (500 mL), and after the mixture was heated to 80 °C, *p*-TSA·H_2O was added (51 mg, 0.268 mmol, 1%). The mixture was subsequently refluxed in a Dean−Stark apparatus for 160 min, cooled to room temperature, and poured into 5% aqueous $NaHCO_3$ (200 mL). The organic layer was dried with Na_2SO_4. The slightly yellow solid, obtained after filtration and removal of the volatiles, was dissolved in *n*-hexane/CH_2Cl_2 (2/1) and purified by chromatography on silica gel (150 mL, eluent: *n*-hexane) resulting in 3.68 g of **5** (23.9 mmol, 89%) as a white solid.

R_f: 0.55 (*n*-hexaan/Et_2O 95:5); mp = 99−100 °C; ^{1}H NMR (300 MHz, $CDCl_3$) δ (ppm) = 3.45 (dd [app. t], J = 1.9, 1.9 Hz, 4H), 6.60 (dt, J = 5.7, 1.9 Hz, 2H), 7.10 (dt, J = 5.7, 1.9 Hz, 2H), 7.34 (s, 2H); ^{13}C NMR (75 MHz, $CDCl_3$) δ (ppm) = 39.0 (CH_2), 119.8 (CH), 130.0 (CH), 134.1 (CH), 137.5 (C), 142.0 (C); MS (*m*/*z*, %) 154 (71, M^+), 153 (100), 152 (42), 76 (33); IR (KBr) 3054, 2898, 2882, 1624, 1430, 1394, 1384, 1313, 1118, 962, 916, 794, 704 cm^{-1}. Anal. Calcd for $C_{12}H_{10}$: C, 93.46; H, 6.54. Found: C, 93.21; H, 6.72.

(−)$_{365}$-(1*R*,2*S*,7*S*,8*R*)-1,2,7,8-Di-epoxy-3,6-dihydro-*as*-indacene (3). 4-Methylmorpholine *N*-oxide (381.5 mg, 3.26 mmol, 5 equiv) and Mn-(*R*,*R*)-Salen (20.7 mg, 0.033 mmol, 5%) were dissolved in CH_2Cl_2 (7.5 mL), after which the mixture was cooled to −78 °C. Diene **5** (100.6 mg, 0.65 mmol) was added at −78 °C, and, after dissolution, *m*-CPBA (∼90% purity, 378 mg, 2.0 mmol, 3 equiv) was added in one portion. After 110 min, 1 N aqueous NaOH (2 mL) was added, and the mixture was then poured into 1 N aqueous NaOH (8 mL) and CH_2Cl_2 (10 mL). The organic layer was washed with saturated aqueous $NaHCO_3$ (10 mL), followed by saturated aqueous NaCl (20 mL). The combined H_2O layers were extracted with CH_2Cl_2 (2 × 20 mL). The combined organic layers were dried on Na_2SO_4, filtered, concentrated, and filtered over silica gel (2 mL, pretreated with a CH_2Cl_2/1% NEt_3 mixture). This resulted in 128 mg of a pale yellow solid. The product was recrystallized from toluene to obtain 93 mg of a white solid **3** (0.50 mmol, 77%, >98% ee, >98% de). The product can be sublimated at 150 °C/0.2−0.3 mmHg.

Sublimation >200 °C, $[\alpha]_D^{25} = -0.8$, $[\alpha]_{365}^{25} = -128.6$ (c = 0.99, $CHCl_3$). ^{1}H NMR (500 MHz, $CDCl_3$) δ (ppm) = 2.99 (dd, J = 17.5, 2.7 Hz, 2H), 3.20 (d, J = 17.5 Hz, 2H), 4.18 (dd [app. t], J = 2.7, 2.7 Hz, 2H), 4.47 (dd, J = 2.7, 0.9 Hz, 2H), 7.12 (2H, s) ppm; ^{13}C NMR (75 MHz, $CDCl_3$) δ (ppm) = 34.3 (CH_2), 57.2 (CH), 58.2 (CH), 125.9 (CH), 137.9 (C), 141.9 (C); MS (*m*/*z*, %) 186 (100, M^+), 158 (50), 130 (72), 129 (60), 128 (68), 115 (58). Analysis on Chiralcel OD-H column, see Supporting Information. IR ($CDCl_3$) 3050, 2914, 2252, 1459, 1420, 1367, 1231, 1207, 1037, 1005, 983, 910, 831, 808, 753, 714, 622 cm^{-1}; HRMS found $[M + H]^+$, 187.0761; calculated for $C_{12}H_{11}O_2$, 187.0758. Anal. Calcd for $C_{12}H_{10}O_2$: C, 77.40; H, 5.41. Found: C, 77.31; H, 5.50.

IR/VCD Spectroscopy. The IR and VCD spectra for (+)-**2** and (−)-**3** are recorded in a demountable cell with KBr windows and a 105 μm spacer. The spectra for (+)-**1** were recorded in a CaF_2 cell with a 200 μm spacer. The unpolarized IR absorbance spectra were recorded at a resolution of 4 cm^{-1}, and the VCD spectra[24] were recorded at a resolution of 6 cm^{-1}. To improve the VCD S/N ratio, an 1830 cm^{-1} long wavepass filter is used.

The collection time for the VCD spectrum was 2 h each, in 4 blocks of 30 min. (+)-**1** was dissolved in $CDCl_3$ at a concentration of 0.11 M. For (+)-**2**, $CDCl_3$ was used as solvent at a concentration of approximately 0.19 M. (−)-**3** was dissolved in $CDCl_3$ at a concentration of 0.20 M.

To obtain a good estimate for the baseline artifacts, one usually measures the VCD of the racemic mixture or both enantiomers.[25] As these are not always available, the VCD of the solvent, measured in the same conditions as the sample, is often a good approximation. In this study, a racemic mixture is only available for **1**. For (±)-**1**, the VCD is measured at the exactly the same conditions as the solvent and the enantiopure solution. In Figure S13 (Supporting Information), the racemic and solvent corrected spectra are given. No significant differences can be seen involving the signs of any peaks.

Computational Methods. Because VCD spectra are composed from all contributions of the different conformations, a conformational search has to be performed. In the scope of absolute configuration (AC) determination by VCD, this is very important because of the strong dependence of VCD on the conformations present.[26]

The conformational landscape is explored by molecular mechanics (MM) as well as with density functional theory (DFT). A systematic search is carried out at the B3LYP/6-31G* level. The aromatic ring of the *as*-hydrindacene skeleton is considered rigid, whereas the attached five-membered rings and exocyclic hydroxyl groups are considered flexible. The dihedral angles are varied in a 60° grid. A bump check and ring constraints[27] ensure that only the chemically sane starting structures are minimized on the B3LYP/6-31G* level.

Also, a systematic search (with a 10° dihedral grid) is performed with MMFF[28] supplemented with a MM3 stochastic search[29] to identify possible further minima. The located MMFF and MM3 geometries are then optimized at the B3LYP/6-31G* level and supplemented with these found from the B3LYP/6-31G* systematic search.

The DFT calculations are performed with Gaussian 03 revision B05[30] in a distributed computing environment. The B3LYP[31,32] functional is used together with the 6-31G* and cc-pVTZ basis sets. Eight additional functionals (B1LYP,

(24) The VCD spectra were recorded on a Bruker IFS 66/S FTIR interferometer coupled to a Bruker PMA37 VCD module. This VCD setup is further specified in: Urbanova, M.; Setnicka, V.; Volka, K. *Chirality* **2000**, *12*, 199−203.

(25) Nafie, L. A. *Appl. Spectrosc.* **2000**, *54*, 1634−1645.

(26) Polavarapu, P. L. *Spectroscopy* **1994**, *9*, 48−55.

(27) Sadowski, J.; Schwab, C. H.; Gasteiger, J. 3D structure generation and conformational searching. In *Computational medicinal chemistry for drugs discovery*; Bultinck, P., De Winter, H., Langenaeker, W., Tollenaere, J. P., Eds.; Marcel Dekker: New York, 2004; pp 151−212.

(28) Halgren, T. A. *J. Comput. Chem.* **1996**, *17*, 490−519.

(29) Allinger, N. L. MM3 version, 1996.

(30) Frisch, M. J.; Trucks, G. W.; Schlegel, H. B.; Scuseria, G. E.; Robb, M. A.; Cheeseman, J. R.; Zakrzewski, V. G.; Montgomery, J. A., Jr.; Stratmann, R. E.; Burant, J. C.; Dapprich, S.; Millam, J. M.; Daniels, A. D.; Kudin, K. N.; Strain, M. C.; Farkas, O.; Tomasi, J.; Barone, V.; Cossi, M.; Cammi, R.; Mennucci, B.; Pomelli, C.; Adamo, C.; Clifford, S.; Ochterski, J.; Petersson, G. A.; Ayala, P. Y.; Cui, Q.; Morokuma, K.; Malick, D. K.; Rabuck, A. D.; Raghavachari, K.; Foresman, J. B.; Cioslowski, J.; Ortiz, J. V.; Stefanov, B. B.; Liu, G.; Liashenko, A.; Piskorz, P.; Komaromi, I.; Gomperts, R.; Martin, R. L.; Fox, D. J.; Keith, T.; Al-Laham, M. A.; Peng, C. Y.; Nanayakkara, A.; Gonzalez, C.; Challacombe, M.; Gill, P. M. W.; Johnson, B. G.; Chen, W.; Wong, M. W.; Andres, J. L.; Head-Gordon, M.; Replogle, E. S.; Pople, J. A. *Gaussian 98*, revision B.05; Gaussian, Inc.: Pittsburgh, PA, 1998.

(31) Becke, A. D. *J. Chem. Phys.* **1993**, *98*, 5648−5652.

(32) Lee, C. T.; Yang, W. T.; Parr, R. G. *Phys. Rev. B: Condens. Matter* **1988**, *37*, 785−789.

B3LYP, B3P86, B3PW91, B98, BHandH, BHandHLYP, MPW1PW91, PBE1PBE)[33] were employed using the 6-31G* basis set.

The agreement between spectra is expressed via the similarity measures given in eqs 1 and 2. The normalized overlap in eq 1 has been discussed earlier.[7]

$$S = \frac{\int f(\sigma\nu)g(\nu)\,\mathrm{d}\nu}{\sqrt{\int f^2(\sigma\nu)\,\mathrm{d}\nu \int g^2(\nu)\,\mathrm{d}\nu}} \tag{1}$$

$$S_{\mathrm{fg}} = \frac{\int w_{\mathrm{fg}}(r)c_{\mathrm{fg}}(r)\,\mathrm{d}r}{\sqrt{\int w_{\mathrm{ff}}(r)c_{\mathrm{ff}}(r)\,\mathrm{d}r \int w_{\mathrm{gg}}(r)c_{\mathrm{gg}}(r)\,\mathrm{d}r}} \tag{2}$$

with

$$w_{\mathrm{fg}} = 1 - \frac{|r|}{l} \leftrightarrow |r| < l$$

$$w_{\mathrm{fg}} = 0 \leftrightarrow |r| \geq l$$

and

$$c_{\mathrm{fg}} = \int f(\nu)g(\nu + r)\,\mathrm{d}\nu$$

The simple overlap is less robust because of the fundamental difference between experimental and simulated spectra. Although the theoretical frequencies are scaled linear to correct for the harmonic approximation and basis set incompleteness, some peaks can still be shifted with respect to their corresponding experimental peak. A similarity measure that takes into account the neighborhood around the peaks results in a more accurate and precise measure for their similarity.

Equation 2[34] allows one to take into account the neighborhood with a width of $-l$ and $+l$ around each point in the spectrum.

Theoretical Spectra. The dipole and rotational strengths are calculated for each DFT minimum on the potential energy surface. The results are single conformer line spectra, which are broadened using a Lorentzian band-shape. Throughout the paper, Lorentzian broadening is always accomplished at a fwhm of 10 cm^{-1}.

Each minimum contributes to the total spectrum in a Boltzmann weighted manner. Conformational populations are based on the free energy. The enthalpy and free energy are calculated under the usual assumptions using standard thermochemical expressions.[35] Appropriate frequency scale factors are used to correct for the harmonic approximation.

Acknowledgment. K.V. is a Research Assistant of the Fund for Scientific Research−Flanders (Belgium) (F.W.O.−Vlaanderen). The F.W.O. is thanked for financial help toward the spectroscopic equipment and the computational facilities used in this study.

Supporting Information Available: ^{1}H NMR and ^{13}C NMR spectra of new compounds **3** and **5**, ^{13}C NMR and synthetic procedure for known compounds **1**, **2**, and *meso*-**1**. Chiralcel OD-H chromatograms demonstrating enantiomeric and diastereomeric purity. General experimental methods. Experimental IR/VCD spectra for **1**, **2**, and **3** and Lorentzian fit. Neighborhood similarity measure for different functionals with IR/VCD experiment. Cartesian coordinates for the optimized structures for compounds **1**, **2**, and **3** and their total energies. Cartesian coordinates for the optimized structure for the **2** conformation eG′ interacting with $CHCl_3$. Tables with calculated and Lorentzian fitted experimental dipole and rotational strengths for the 6-31G* and cc-pVTZ basis sets. This material is available free of charge via the Internet at http://pubs.acs.org.

JO050666H

(33) Frisch, A. E.; Frisch, M. J.; Trucks, G. *Gaussian 03 User's Reference*; Gaussian, Inc.: Pittsburgh, PA, 2003.

(34) De Gelder, R.; Wehrens, R.; Hageman, J. A. *J. Comput. Chem.* **2001**, *22*, 273−289.

(35) McQuarrie, D. A. *Statistical Thermodynamics*; Harper and Row: New York, 1973.